Composites: Part A 149 (2021) 106548

Contents lists available at ScienceDirect

Composites Part A

journal homepage: www.elsevier.com/locate/compositesa

Non-tensile piezoresistive sensor based on coaxial fiber with magnetoactive shell and conductive flax core

Quan Shu [a], Tao Hu [a], Zhenbang Xu [b], Junshuo Zhang [a], Xiwen Fan [a], Xinglong Gong [a,*], Shouhu Xuan [a,*]

[a] CAS Key Laboratory of Mechanical Behavior and Design of Materials, Department of Modern Mechanics, CAS Center for Excellence in Complex System Mechanics, University of Science and Technology of China (USTC), Hefei 230027, China

[b] CAS Key Laboratory of On-orbit Manufacturing and Integration for Space Optics System, Changchun Institute of Optics, Fine Mechanics and Physics, Chinese Academy of Sciences, Changchun 130033, Jilin, China

ARTICLE INFO

Keywords:
A. Fiber
B. Mechanical properties
B. Magnetic properties
Piezoresistive sensor

ABSTRACT

Flexible and wearable sensors have been widely applied in smart monitoring and electronic devices. However, the piezoresistive sensor with high strength and tunable sensing modes remains a challenge. Here, a flexible and magnetically response piezoresistive sensor consisting of silver nanowires (AgNWs) coated flax fiber (FF) as the electronic core (AF) and magnetorheological elastomer (MRE) as the packaging shell (MAF) was developed. Due to good flexibility and magnetic characteristic of MRE shell, MAF sensor is sensitive to the bending stimuli and magnetic field. Furthermore, D-MAF sensor with dual conductive flax fiber which exhibited superb mechanic-electric properties can be constructed. The relative resistance variation ($\Delta R/R_0$) of D-MAF sensor reaches 19.8% under bending angle of 16.2°. Sensors exhibit unique non-tensile behavior, its mechanic-electric–magnetic nature is mainly originated from the piezoresistive performance. The piezoresistive sensor shows excellent mechanical properties thus demonstrating a broad promising in future intelligent devices, like artificial skins and soft robotics.

1. Introduction

During the past decades, the flexible and wearable sensors have been widely applied in flexible robots [1–3], smart monitoring [4,5], magnetic actuator [6,7], artificial skin [8,9], and electromagnetic absorber [10–12]. Among them, the flexible sensors mainly contain transistor [13,14], capacitive [15,16], piezoelectric [17,18], and piezoresistive [19,20] sensors. Various methods have been proposed to fabricate highly sensitive flexible piezoresistive sensors which showed fast response, high sensitivity and excellent durability [21]. Because of the facile fabrication, integration and real-time signal collection, the piezoresistive sensor has a great advantage in modern wearable devices [22,23]. Generally, most of the piezoresistive sensor has high elasticity and low strength due to the soft matrix. However, the weak strength limits their practical application, thus many efforts have been done to improve the carrying matrix. Recently, it is found that the fiber reinforced matrix can extensively improve the performance of piezoresistive sensor. Besides the highly strengthened mechanical properties, the flexible sensors also possess fast response electrical characteristics thus show high potential in electronic skin, wearable devices, and smart robots [24].

Among various structured sensor, the flexible fiber-like ones attract increasing interests due to their large tension performance, high sensitivity and good durability [25]. In recent years, fiber sensors are mainly used in artificial skin, artificial hair, intelligent and structural monitoring [26–29]. Generally, the flexible fiber-like sensors mainly include single fiber sensors [30,31]. Single fiber-like sensors based on soft matrix often exhibited good mechanical properties, high stability and flexibility [26,28]. Because of the high conductivity, fast response and ultrahigh elasticity, single fiber-like sensors composed of conductive materials have attracted much more attention [32,33]. Georgopoulou et al fabricated a fiber sensor by 3D printing a fused deposition modelling filament based on conductive thermoplastic polyurethane and a styrene block copolymer compound [34]. However, due to the low strength of these kind of fibers, the development and application of this type sensor are limited. Recently, single fiber sensors made from non-natural fibers such as carbon and Kevlar fibers combined with soft substrates have been widely used in soft robots and intelligent perception [35–37].

* Corresponding authors.
E-mail addresses: gongxl@ustc.edu.cn (X. Gong), xuansh@ustc.edu.cn (S. Xuan).

https://doi.org/10.1016/j.compositesa.2021.106548
Received 13 April 2021; Received in revised form 27 June 2021; Accepted 1 July 2021
Available online 6 July 2021

Nevertheless, the high cost of these non-natural fibers has brought trouble to the research and practical engineering.

Natural fiber, such as flax fiber, cotton, and hemp fiber, have the advantages of environment protection, low cost and simple preparation. It is found that these natural fibers can be widely used as template for high performance sensor and other smart applications [38–41]. Especially, the encapsulation-free piezoresistance sensors could be fabricated based on the resilient graphited knitting hemp fibers and the product exhibited a low-detection-limit and a high permeability [41]. Obviously, the piezoresistance sensor based on high strength natural fiber is favorable to overcome the critical issues in traditional elastic fiber-like sensors. During the past few decades, most of the sensors based on flexible matrix and strengthen fiber have been focused on the tensile or bending sensing behavior, multi-functional natural fiber sensors that can respond to different stimuli are still scarce. Due to the high strength, good biocompatibility, excellent weavability and ultrahigh bending ability, flax fiber has become an ideal candidate for the multi-functional piezoresistive sensors. As a result, it has become a meaningful work to explore the multi-mode piezoresistive sensors based on flax fiber.

In this work, a non-tensile coaxial piezoresistive fiber sensor with force sensing and magnetic response properties was developed. The conductive flax fiber was employed as the core, in which the silver nanowires (AgNWs) interwoven-stacked on flax fiber constituted conductive network, and magnetorheological elastomer (MRE) was the soft shell. As piezoresistive sensors, the conductive fiber exhibited ideal flexibility, stability and sensing performance and they can be used to monitor the movements of various human joints. Owing to the high strength of the flax fiber, the present fiber sensor is non-tensile and it can sensitive to stress and magnetic field. Additionally, the multi-functional D-MAF sensors with different external shapes can be deflected at ranging angles under the magnetic field, thus act as both magnetic field actuator and sensors. Moreover, the conductive flax fibers have been further woven into a three-dimensional network structure to perceive external pressure stimulation and feedback with electric signals in real time.

2. Experimental section

2.1. Materials

Flax fibers (4 strands of fibers per centimeter) were supplied from Jiujiang Yarnfan Textile Co. Ltd, China. The PDMS (type Sylgard 184) precursor and curing agent were purchased from Dow Corning GmbH, USA. Carbonyl iron particles (CIPs, type CN) with an average diameter of 3.85 μm from BASF were used as ferromagnetic particles. The raw material for self-prepared silver nanowires (AgNWs) solution [30,42] contained Polyvinylpyrrolidone (PVP), $AgNO_3$, glycerol, ethanol and NaCl were from Sinopharm Chemical Reagent Co., Ltd.

2.2. Experiments

The flax fiber (FF) was immersed into the deionized water for 5 min and then soaked into the ethanol solution for 15 min after dried in the oven. FF was immersed into the AgNWs solution and treated under ultrasonication for 1 min, and then dried in the oven at 60 °C for 10 min. By repeating the dip-coating procedure for several times, the AgNWs-FF (AF) with high conductivity was obtained. For a single AF, copper wires were adhered to both the ends of AF by silver conductive paint to test the electrical properties. Then, MRE precursor (PDMS curing ratio of 20:1, CIPs mass fraction of 50 wt%) was prepared by stirring the mixture for 5 min, and then vacuum treated for 10 min to remove the bubbles. The AF was encapsulated with magnetorheological precursor (PDMS/CIPs mixture) in the molds with different shapes.

For convenience, the composite MREs with single AgNWs-flax fiber (AF) were defined as MAF. Simultaneously, MAF with dual AF (D-AFs) series connection were defined as D-MAF, where D meant dual. The D-MAF with triangular cross section was defined as TD-MAF, as well as the square cross section was defined as SD-MAF. The length and radius of MAF and D-MAF was 65 mm and 1.5 mm, respectively. The length and triangular cross section length of TD-MAF was 65 mm and 10 mm, respectively. The length and rectangular cross section length of SD-MAF was 65 mm and 9 mm, respectively.

With the completion of the absorption, the as-prepared AF was fully immersed in MR precursor using the cylindrical mold. After curing in an oven at 90 °C for 30 min, the CI/PDMS shell was uniformly coated on the conductive Ag-Flax fiber core to form the MAF (Fig. 1a). As for dual AF (D-AF), one end of two AFs was connected through copper wires and silver conductive paint (Fig. 1b). Fig. 1c shows D-AF was encapsulated by a cylindrical mold to form a tunable multi-mode D-MAF sensor. Meanwhile, the optical images of MAF and D-MAF are presented, and the cross-section image of D-MAF is displayed (Fig. 1d). Due to the weavability of conductive fibers, single fiber can be assembled to form dual conductive fibers and woven into fabric network structure, which can be further applied to realize wearable multi-mode flexible sensors (Fig. 1e).

2.3. Characterization

The microstructure of the flax fiber (FF), conductive AgNWs-flax fiber (AF), MAF and D-MAF were observed by scanning electron microscope (SEM, Philips of Holland, model XL30 ESEM-TMP) under 3 kV. The hysteresis loop of isotropic MRE (CIPs mass fraction of 50%, PDMS curing ratio of 20:1) and MAF were tested by Hysteresis Measurement of Soft and Hard Magnetic Materials (HyMDC Metis, Leuven, Belgium). The rheological properties of anisotropic and isotropic MREs, and MAFs were measured by a commercial rheometer (Physica MCR 302, Anton Paar Co., Austria). The tensile tests were completed by a universal testing machine (MTS criterion 43, MTS System Co., America). The bending test system consists of a dynamic mechanical analyzer (DMA, ElectroForce 3200, TA instruments, Minnesota 55344, USA) and Modulab MTS (Solartron analytical, AMETEK advanced measurement technology, Inc., United Kingdom). The magnetically response tests were finished by Modulab MTS and a DC power electromagnetic coil. The infrared thermal camera (type Image IR 8300, Germany) was used to obtain the thermal images. In order to ensure the accuracy of the experiment results, the MAF and D-MAF were adhered to the PDMS film, and the ends of the PDMS film were clamped with DMA for bending test.

3. Results and discussion

3.1. Microstructures and properties of AgNWs, AgNWs-flax fiber, MAF and D-MAF

Fig. 2a shows the SEM image of flax fiber after pretreatment. AgNWs and flax fiber were tightly combined to form a woven conductive fiber after the dip-coating process. The SEM images of AF and as-prepared AgNWs were shown in Fig. 2b and Fig. S1a, respectively. Clearly, the AgNWs with the length of 500 nm showed stable structure and were firmly combined with each strand of flax fibers (Fig. S1a). The as-prepared MAF exhibited the typical core shell structure, which was comprised of silver/flax fiber core and the MRE shell (Fig. 2c). AF was well embedded in the center of the matrix, showing the core–shell structure (Fig. S1b). Each strand of fiber interacted with the matrix, thus significantly enhanced the matrix structure and improved the mechanical properties of MRE (Fig. 2d). The magnified image shows the PDMS/CI polymer firmly adhered to the fiber, ensuring good mechanical properties of MAF (Fig. 2e). After the core–shell structures were formed, the conductive path of AgNWs was well protected from undesired leaching (Fig. 2f). The MRE matrix surrounded and wrapped the D-AFs, and the two fibers were separated by the substrate to form a core–shell structure with D-AFs as the core (Fig. 2g).

Due to the excellent conductivity, the AgNWs were employed as conductive fillers in sensors [42]. Because of the AgNWs network on the

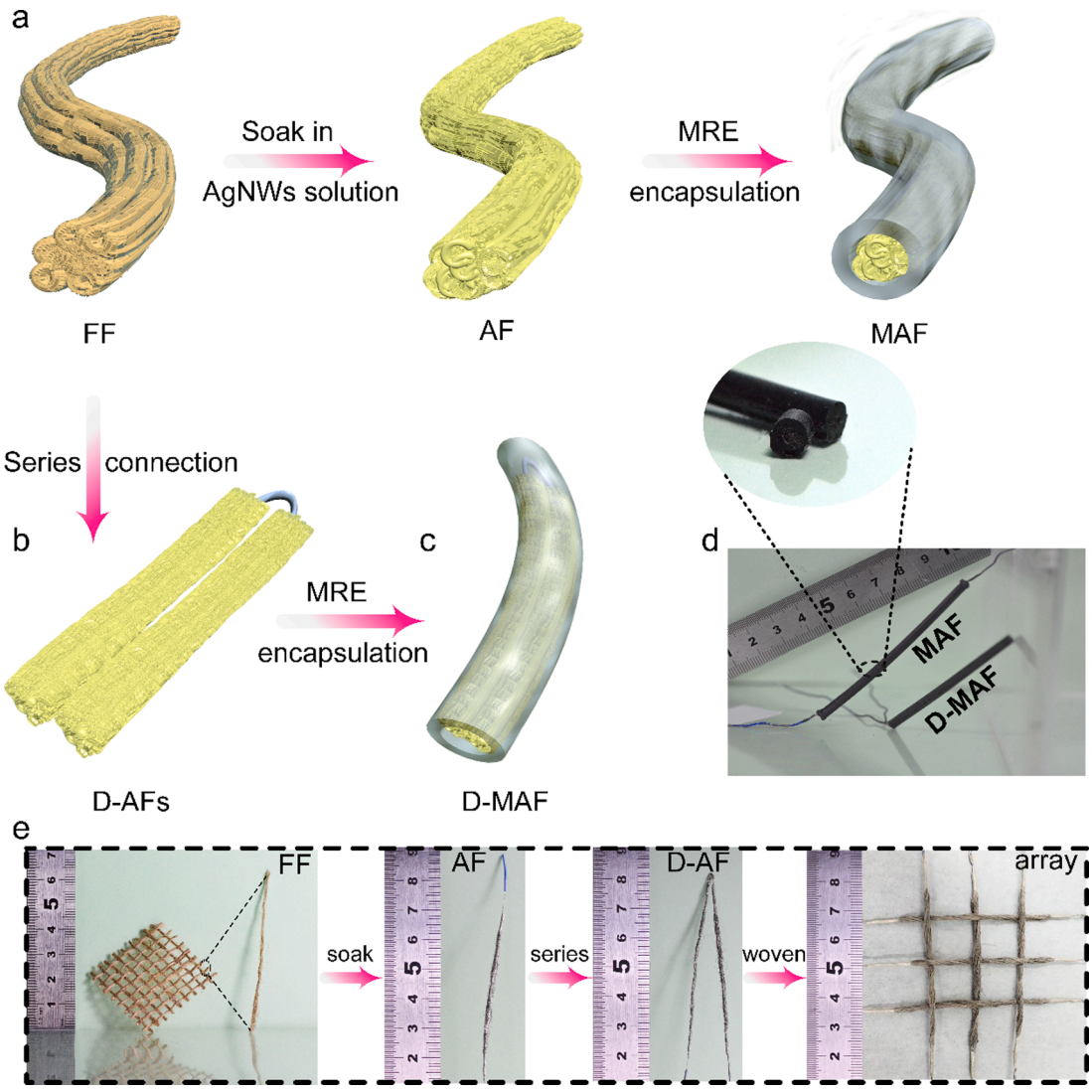

Fig. 1. Preparation process of (a) single MAF, (b) dual AFs and (c) D-MAF; (d) The image of MAF and D-MAF; (e) Optical images of flax fiber, AF, D-AFs, and sensing array. (For interpretation of the references to colour in this figure legend, the reader is referred to the web version of this article.)

flax fiber, the MAF is conductive and the electrical performance can be demonstrated by lighting the LED bulb (Fig. S1d). Different from most of the previously reported conductive materials [3,10–12], the AgNWs coated flax fiber showed high mechanical properties thus can be applied as the non-tensile bending sensor. The flexible MAF and D-MAF exhibited superb electrical conductivity characteristics. D-AFs were separated from each other without entanglement, which ensured the stable electrical properties of D-MAF. The enlarged area of Fig. 2g showed that D-AFs were completely embedded within the MRE matrix (Fig. S1c). AgNWs were attached to each strand of fiber to ensure the conductivity (Fig. 2h). It can be clearly found that the silver content of AgNWs on the AF surface was as high as 49.9 wt% (Fig. 2i). As a kind of natural wood fiber, there are many burrs on the surface of flax fiber. In the preparation, the MRE could stabilize the conductive network on fiber bundles and eventually formed a complete shell on the core structure. As shown in Fig. 2e, the substrate was tightly adhered onto the surface of fiber bundles. Here, the AgNWs were firmly sandwiched between MRE and flax fiber, which enable them to be applied in piezoresistive sensors. Therefore, the defects and holes in the matrix were caused by the surface burrs of the fiber, but they do not affect the mechanical enhancement effect of flax fiber on MAF and the electrical performance of the sensor. As a result, MAF still maintained good conductivity and favorable stability during the encapsulation process.

Due to the existence of the magnetic CIPs, shear storage modulus of MAF increases with the magnetic field. In comparison to the isotropic MRE (MRE) and anisotropic MRE (An-MRE), the shear storage modulus of MAF is obviously higher (Fig. 3a). The strengthening effect must be responded for the staggered structures formed by the AF and MRE matrix, which significantly enhanced the mechanical properties of the composite. Meanwhile, the tensile properties of pure flax fiber, AF, isotropic MRE and MAF were tested. As shown in Fig. 3b, the fracture forces of flax fiber, AF, MAF and isotropic MRE were 42.5 N, 35.1 N, 22.4 N and 2.3 N, respectively. Flax fiber was a kind of natural fiber composed of multiple groups of fiber bundles with good hydrophilicity. After the absorption, the AgNWs network adhered on the fiber bundles of the AF, which reduced the interaction between them after soaking for many times. Therefore, the mechanical properties of the flax fiber were weakened. Moreover, flax fiber enhanced the strength of MAF due to its good mechanical property. In the tension process, the tensile force would be mainly concentrated on the non-tensile flax fiber. MRE shell was first fractured and broken during the stretching process, while the flax fiber was not completely broken. The fracture force of MAF was almost 10 times than isotropic MRE, which indicated that the combination of MRE matrix and AF remarkably improved the tensile strength.

MAF exhibits unique magnetization performance because CIPs are soft magnetic materials with low remanence and coercivity. As shown in

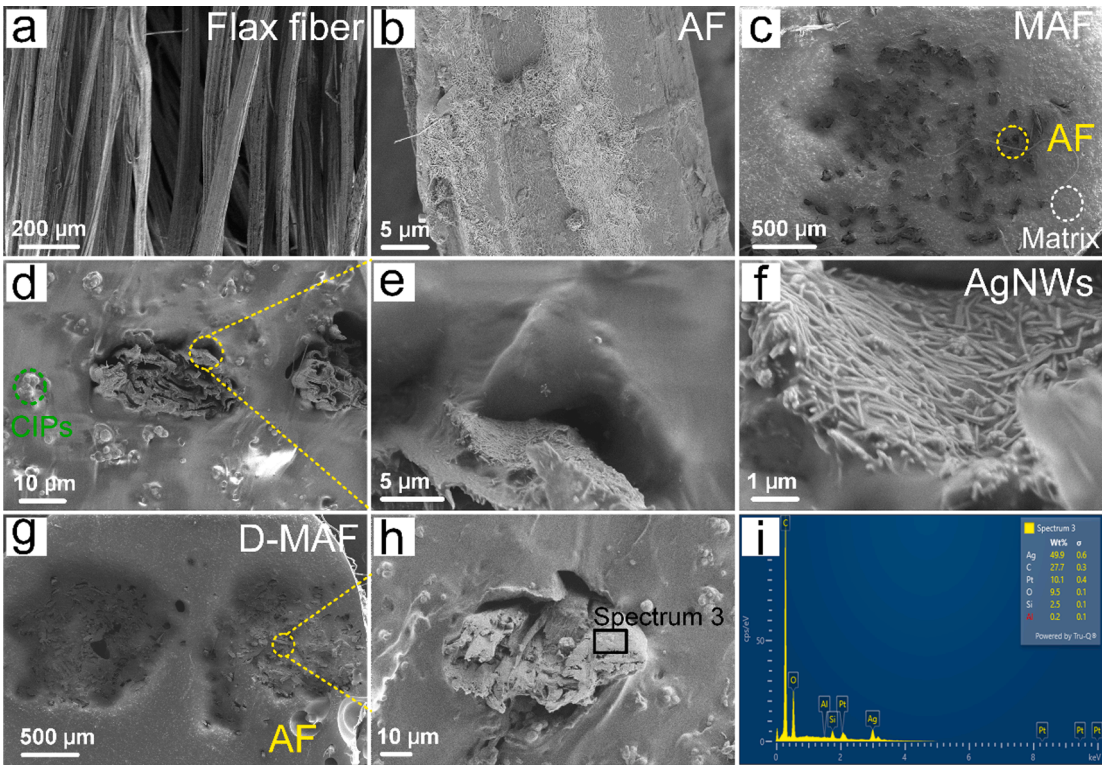

Fig. 2. SEM images of (a) flax fiber, (b) AgNWs-flax fiber and (c) MAF; The cross section of (d) MAF; The microstructure of (e) MAF composition and (f) AgNWs; The cross section of (g) D-MAF and (h) enlarged AF; (i) Element analysis of AgNWs. (For interpretation of the references to colour in this figure legend, the reader is referred to the web version of this article.)

Fig. 3c, the hysteresis loops of isotropic MRE and MAF were similar. The saturation magnetizations (M_s) of isotropic MRE and MAF were 104.7 emu/g and 85.8 emu/g, respectively. The M_s of MAF was smaller than MRE due to the lower mass fraction of CIPs in MAF. Moreover, the more times of dip-coating, the higher mass fraction of AgNWs and the lower resistance of AFs (Fig. 3d). Meanwhile, the inset images showed the contact area among the AgNWs also significantly increased and more stable conductive network structures were formed, which effectively improved the conductivity.

3.2. Non-tensile bending responsive properties of MAF and D-MAF

Due to the high toughness of flax fiber, the MAFs showed good bending elasticity and high tensile strength. The electrical properties of MAF were highly dependent on the AgNWs network. Because the conductive network structure under the external excitation has good recoverability, MAF can be employed as a sensor. Here, Cu wires were connected to both ends of MAF through conductive silver paste, and the electro-mechanical performances of the MAF sensor under different bending angles were researched. Before the bending test, the tensile-electrical performance of the MAF was conducted (Fig. 4b). As the low tensile strain was applied, the relative resistance of MAF remained substantially unchanged due to the inherent stiffness and low ductility of the flax fiber. As we know, the traditional elastic fiber sensor is sensitive to both the tensile and bending, thus it is very difficult to decouple the different stimuli. Here, our prepared flax fiber was non-tensile, thus it can solely respond to the bending stimuli. The presence of flax fiber also highly strengthened the final sensor to resist the large external stress. Under a high tensile stress, the relative resistance of MAF significantly increased when the matrix was broken and the surface was damaged (Fig. 4a).

During the test, MAF sensor was fixed with the clamps of DMA, and tested under bending with cyclic sine waveform (Fig. 4c). The resistance variation was defined as $\Delta R = R - R_0$, where R_0 was the initial resistance. As shown in Fig. 4d, the mechanical electrical performance of MAF under bending angle varied from 3.2° to 16.2° was investigated, and the test was repeated for three times under each bending angle. The mechanical response of MAF strain sensor was gradually obvious with the increase of bending angle. By keeping the bending angle at 5.5°, the influence of different waveform loading (triangular, square and sine wave) on the electrical performance of MAF sensor was explored (Fig. 4e). MAF strain sensor could distinguish different waveforms well and presented favorable and stable electrical response.

Afterwards, the electrical responses of MAF strain sensor at different frequencies were tested (Fig. 4f). The $\Delta R/R_0$ was 2.7% at 0.1 Hz, 0.5 Hz and 1 Hz under bending angle of 7.1°. The results indicated the properties of MAF strain sensor was hardly affected by the bending frequency. Furthermore, in order to evaluate the sensing performance of MAF, the gauge factor GF_f was calculated by using equation $((\Delta R/R_0)/\Delta\theta)$, in which $\Delta\theta$ was the variation of bending angle (inset of Fig. 4e). Here, GF_f could be divided into two parts (blue and green region) with different tendencies, and the corresponding bending angle was 3.2–8.4° and 8.4–16.2°. The GF_f reached as high as 5.98×10^{-3} and 2.6×10^{-3} in blue and green region after being fitted. Obviously, the MAF showed a better sensitivity at lower bending angles than at high bending angles (Fig. 4g). MAF was more sensitive at small angles and suitable for accurate small deformation ranges. Since the stability of sensing devices was essential in practical application, the sensor was tested by 1000 continuous bending cycles at 0.5 Hz frequency and 7.1° bending angle (Fig. 4h). The results of cyclic bending tests demonstrated that MAF could be employed in sensing devices due to good sensitivity and stability. After bending, MAF could still light the LED bulb, which reflected the good conductivity of the sensor.

Furthermore, the performances of mechanic-electric–magnetic multi-functional response in dual conductive fiber modes were investigated. Here, the electrical performances of D-MAF sensor under bending stimulation and magnetic field were explored, respectively. Similarly,

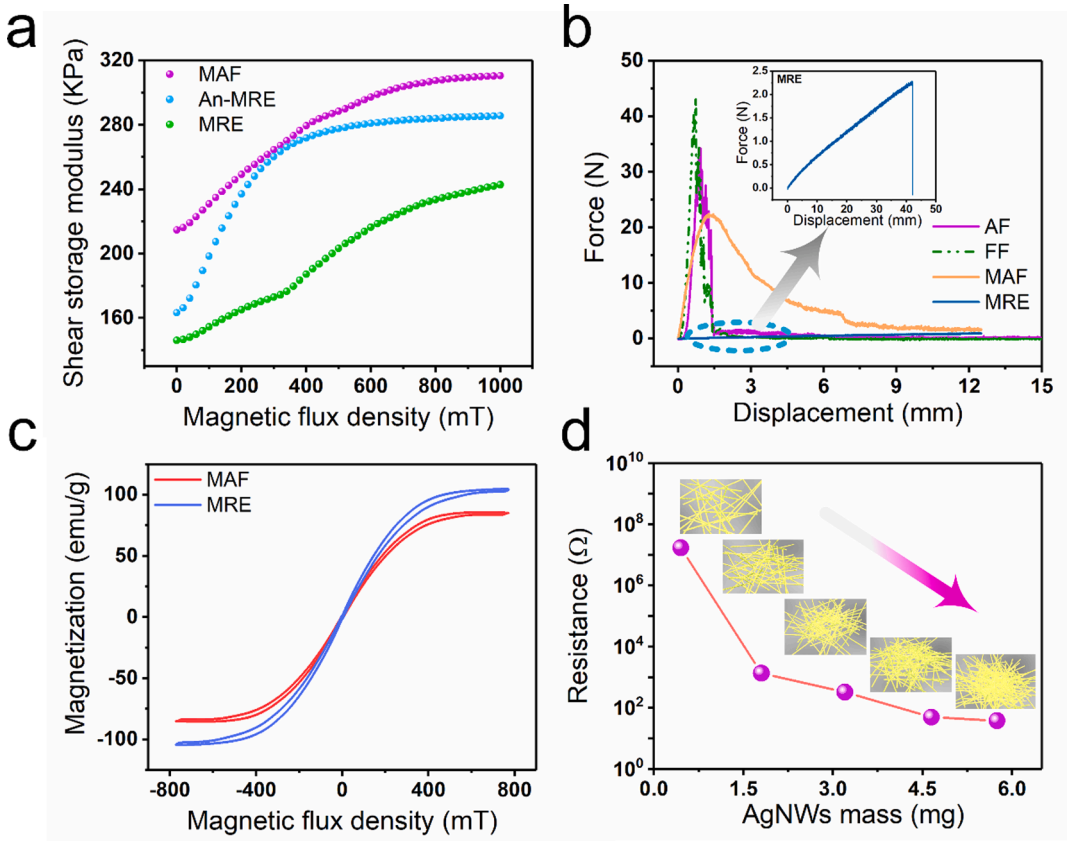

Fig. 3. (a) Rheological properties of MAF, isotropic and anisotropic MRE with 50% CIPs mass fraction; (b) tensile properties of flax fiber (FF), AgNWs-flax fiber (AF), MRE and MAF; (c) saturation magnetization of MRE and MAF; (d) resistance of AF with various AgNWs mass. (For interpretation of the references to colour in this figure legend, the reader is referred to the web version of this article.)

the response of D-MAF sensor to tensile strain was investigated (Fig. S2a). The D-MAF sensor formed in series connection was not sensitive to the tensile response due to the large stiffness and low flexibility. The $\Delta R/R_0$ increased slowly with the crack propagation on the surface of the matrix until the matrix was completely broken. Fig. 5a exhibited the D-MAF sensor variation process images of loading–unloading process. The sensor had superb conductivity during the bending, the $\Delta R/R_0$ varied from 3.8% to 19.3%, and it could return to 3.9% during the gradient unloading process (Fig. 5b). With increasing of the bending angle, the electrical response became more obvious. When the bending angle gradually recovered, the conductivity came back to the original value and the D-MAF sensor showed good stability.

Subsequently, the electric response under different waveforms to D-MAF was investigated (Fig. 5c). Clearly, with the loading of triangular, square and sine waveform, the electrical response of D-MAF sensor accurately reflected the corresponding waveform signal. In the loading and unloading process, the D-MAF sensor showed outstanding and consistent sensitivity (Fig. 5d). With the increase of bending angle, the $\Delta R/R_0$ of D-MAF sensor gradually became significant. As shown in Fig. S2b, the stability of D-MAF was tested by 400 cycles at 11.8°. D-MAF sensor exhibited good electro-mechanical coupling properties and response performance under bending stimuli.

Then, the magnetic-mechanic-electric coupling performances of D-MAF sensor under the external magnetic stimuli were investigated. The influence of the magnetic field on the actuation behavior was investigated. One end was fixed like a cantilever beam, D-MAF was subjected to the magnetic field force. D-MAF sensor showed a classic sensitivity under different magnetic flux density (Fig. 5e). When the applied magnetic field density increased from 40 mT to 80 mT, the $\Delta R/R_0$ of the sensor changed from 8.9% to 15.9%, showed a positive relation. Furthermore, the deflection angle and displacement caused by the magnetic field reflected the unique driving performance of the sensor. As shown in Fig. 5f, the images presented the actuating process of D-MAF sensor. With the magnetic field increased from 40 to 80 mT, the deflection angles varied from 1.7° to 14.1°, indicated the outstanding magnetic actuation sensing characteristics and superior mechanical-electrical-magnetic coupling properties.

3.3. *Actuate-electrical properties of TD-MAF and SD-MAF under magnetic field*

The external morphology of the D-MAF sensor can be controlled by varying the preparation mold, which further influences the actuation performance. The driving behavior of the sensor with different shapes under external magnetic field was explored. Normally, sensors are required to perceive and monitor external stimuli along specified direction and response in time. Based on this special application requirement, the sensor with triangle and square cross section were designed. Originated from the magnetic CIPs, the sensor with PDMS-CIPs used as the shell can be easily magnetized. Therefore, the multi-mode D-MAF sensor could be actuated under the magnetic field and stress, demonstrated a multi-functional sensing and actuation.

Different shell structures can realize variable stiffness and directional deflection of D-MAF. The high flexibility of PDMS matrix and stable conductive properties of AFs endowed TD-MAF sensor with outstanding bending performance and sensing characteristics. By fixing one end as a cantilever beam, the MAF sensor was actuated under the magnetic field (Fig. 6a). Interestingly, the angular sensor could be deflected when the rectangular surface was perpendicular to magnetic field (Fig. 7b). SD-MAF actuating occurred under the magnetic field, the conductive path of the sensor produced some degree of crack damage (Fig. 7a). The images of TD-MAF, SD-MAF and SD-MAF magnetic response are shown

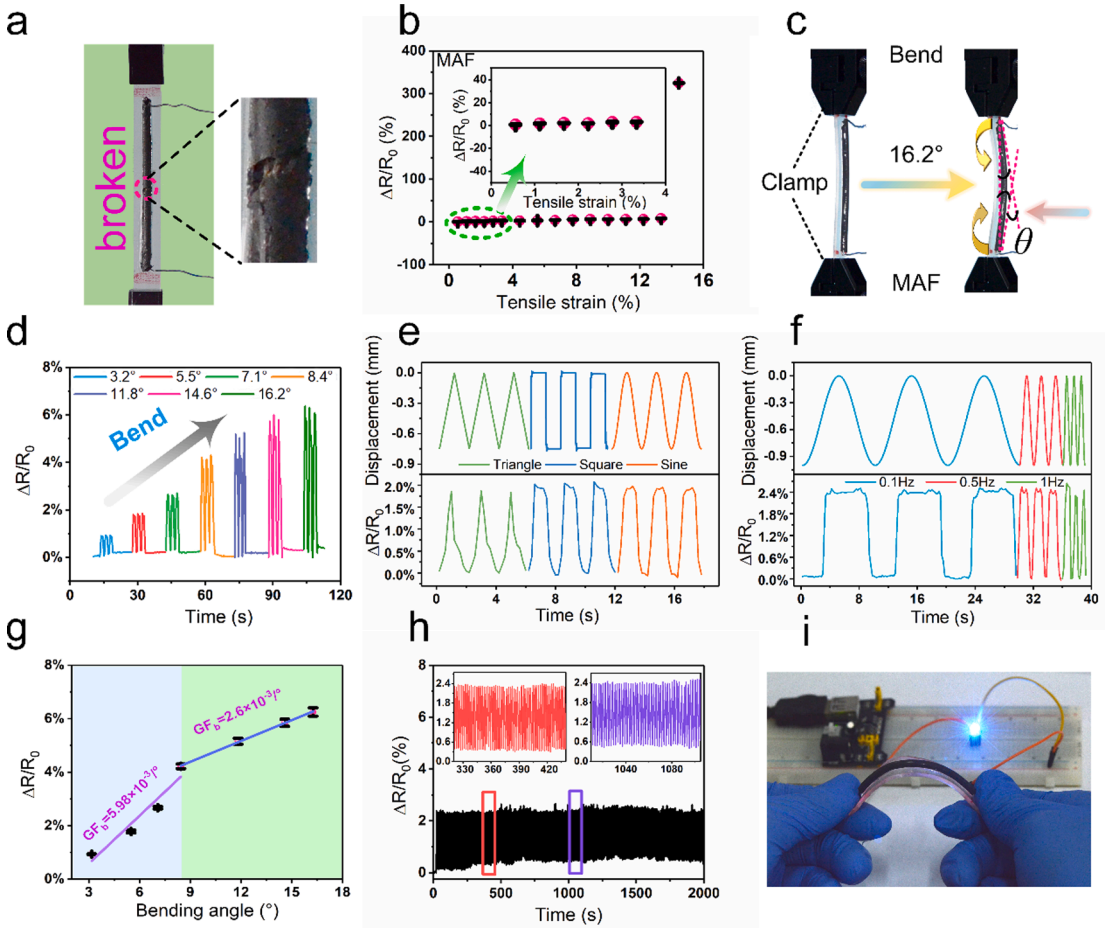

Fig. 4. (a) The image and (b) the $\Delta R/R_0$ of MAF response to tensile strain; (c) The diagram image and (d) the $\Delta R/R_0$ of MAF bending angle 3.2–16.2°; The electrical and displacement response of MAF sensor under bending (e) with cyclic sine, triangle and square waveform and (f) various frequency of 0.1 Hz, 0.5 Hz and 1 Hz; (g) $\Delta R/R_0$ versus bending angle; (h) The stability under 1000 cyclic bending; (i) MAF lighted the LED bulb after bending. (For interpretation of the references to colour in this figure legend, the reader is referred to the web version of this article.)

in Fig. 7c–e, respectively. In contrast, due to the increase in the moment of inertia, the bending rigidity became larger, so it was more difficult to deflect when the edge of the sensor was perpendicular to magnetic field (Fig. 7f–h). The cross section z axis moment of inertia can be approximately estimated as

$$I_z = \int_A y^2 dA \tag{1}$$

where I_z is the moment of inertia, A is the cross-sectional area of D-MAF and y represents the distance to the z axis.

$$I_{zf} = \sqrt{3}a^4/96 \tag{2}$$

$$I_{zg} = a^4/12 \tag{3}$$

$$I_{zh} = a^4 \tag{4}$$

Among them, a is the length of the cross section of the sensor.I_{zf}, I_{zg} and I_{zh} is the moment of inertia of Fig. 7f–h, respectively. By comparison, the result is

$$I_{zh} > I_{zg} > I_{zf} \tag{5}$$

$$\mathrm{K} = EI_z \tag{6}$$

Additionally, K is the bending rigidity and E is the elastic modulus. According to the theoretical calculation results, the larger the bending rigidity, the smaller the deflection angle and driving displacement, which was also consistent with the experimental results.

TD-MAF sensor performed superior actuation-sensing behavior attracted by the variable magnetic field. As shown in Fig. 6b, the $\Delta R/R_0$ of sensor rose from 2.6% to 11.2% with increasing of magnetic field density. Fig. 6d exhibited the driving process of the TD-MAF sensor. The deflection angle and displacement of TD-MAF sensor were gradually raised with increasing of the magnetic field density (Fig. 6c). When the magnetic field density was kept at 50 mT, the driving angle of TD-MAF sensor reached 15.36° and the deflection displacement was 10 mm. After that, driving response experiments were carried out under 20 mT for 400 cycles, and the results indicated the TD-MAF sensor exhibited an excellent stability (Fig. 6e).

The mechanic-electric-magnetic response performances of SD-MAF were also tested. The $\Delta R/R_0$ of SD-MAF sensor heighten significantly by increasing the magnetic field density (Fig. 6f). Similarly, one end of the SD-MAF was fixed like a cantilever beam, the effect on the electrical performance of sensors with different structures under magnetic field was investigated. The driving angles and deflection displacements of SD-MAF sensor gradually enhanced with increasing of the magnetic field density (Fig. 6g). By changing the encapsulation structures and sizes of D-MAF sensor, or increasing the relative magnetic field density, the deflection angle and displacement are simultaneously affected by the magnetic field and encapsulation structures.

3.4. The sensing application of MAF and D-MAF sensors

The bending experiments showed that MAF and D-MAF sensors

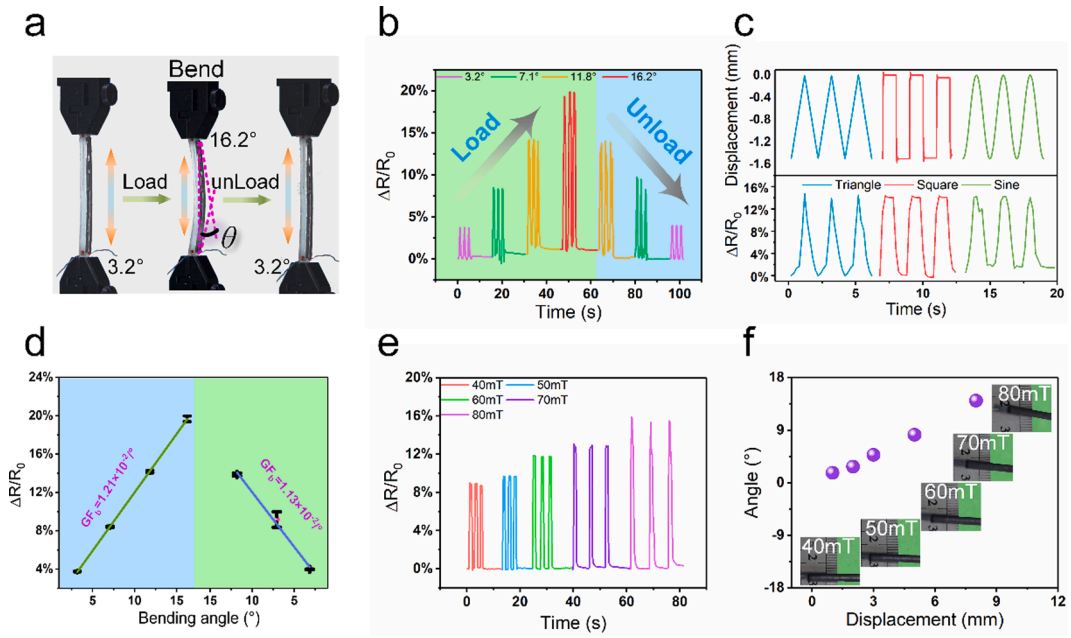

Fig. 5. D-MAF bending angle 3.2–16.2–3.2°: (a) The image and (b) the $\Delta R/R_0$ of D-MAF loading and unloading process; The electrical and displacement response of D-MAF sensor (c) with cyclic sine, triangle and square waveform and (d) $\Delta R/R_0$ versus bending angle under loading and unloading; (e) The electrical response and (f) corresponding deflection angle versus displacement of D-MAF sensor under different magnetic flux intensity. (For interpretation of the references to colour in this figure legend, the reader is referred to the web version of this article.)

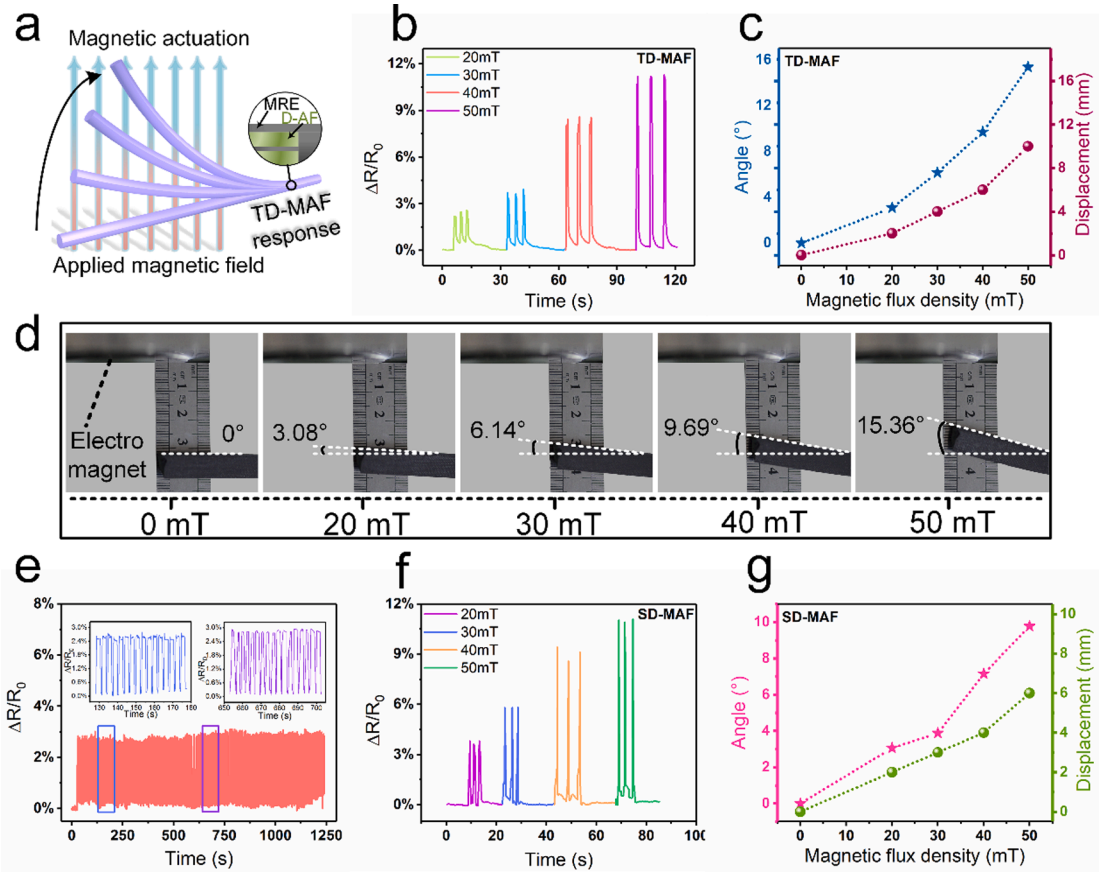

Fig. 6. Different shapes of D-MAF under various magnetic field simulation: (a) Actuation schematic diagram of TD-MAF, (b) the $\Delta R/R_0$ performance, the driving (c) angle versus displacement and (d) optical images of TD-MAF under different magnetic field; (e) The stability of TD-MAF under cyclic actuation at 20 mT magnetic field; (f) The $\Delta R/R_0$ and (g) deflection angle and displacement of SD-MAF sensor under different magnetic fields. (For interpretation of the references to colour in this figure legend, the reader is referred to the web version of this article.)

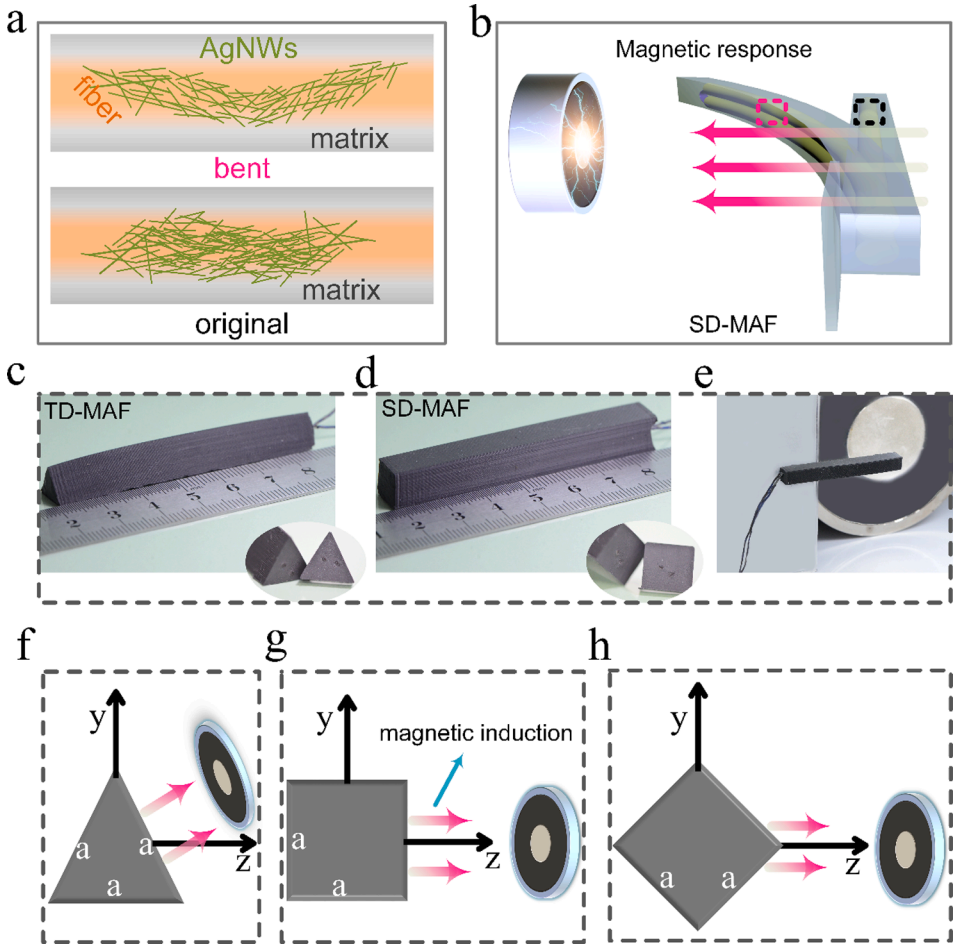

Fig. 7. (a) Schematic illustrations of the SD-MAF bending sensing mechanism; (b) The schematic illustration of D-MAF sensor as a cantilever beam under magnetic field; The images of (c) TD-MAF and (d) SD-MAF; (e) SD-MAF magnetic response optical image; Different surface moment of inertia of (f) TD-MAF and (g, h) SD-MAF. (For interpretation of the references to colour in this figure legend, the reader is referred to the web version of this article.)

possessed both good mechanic-electric–magnetic sensing and actuation performance, and were ideal candidates for flexible sensor and actuator. Here, the AFs were woven into a block fabric network structure and encapsulated by MRE to further illustrate the potential sensing application of AFs. The MRE with the CIPs content of 50 wt% and the dimension of 50 mm × 50 mm × 2 mm was selected as the substrate for 3 × 3 sensor arrays. Fixed the edges of 3 × 3 MRE sensor array, permanent magnet was used to attract the intersection point between the AFs, and finally a cross-shaped route was formed (Fig. 8a).

Because the CI particles in the matrix were attracted by the magnetic field, the AFs and the substrate squeezed each other in the matrix. The $\Delta R/R_0$ at the intersection between the AFs array changed significantly, which fully illustrated the high sensitivity and rapid response of the sensor array (Fig. 8b). The permanent magnet was used to attract the center of the AFs at a fixed point, and the relative magnetic field intensity was changed by moving the magnet (Fig. S7). The $\Delta R/R_0$ varied from 38% to 265%, reflecting the excellent mechanic-electric performance of the sensor array (Fig. S3). Additionally, a 10 g weight was applied at the joint between the AFs and moved in L shape on the matrix surface, and the $\Delta R/R_0$ of the sensor array precisely reflected the corresponding mechanical stimulation (Fig. 8d). This array also can be weaved into clothing for intelligent monitoring (Fig. 8c). Moreover, the light bulb lighting experiment of the sensor array showed that the sensor array kept high conductivity when weaving into a conductive fiber network (Fig. S4). The thermal distribution of the sensor array after electrification was record by using the infrared thermal imager, which clearly showed the electric-thermal coupling performance (Fig. S5).

The conductive path of AFs was retained which showed low resistance and superb conductive characteristics under bending. The conductive mechanism of the sensor under the excitation of bending was analyzed (Fig. S6). The sensing performance of MAF sensors were essentially based on the microstructure change of AgNWs network. When the bending stimuli was applied, the AgNWs embedded in the PDMS-CIPs matrix were stretched and slide. Additionally, the number of AgNWs joints decreased and the distance between AgNWs rose, resulting in the increment of resistance due to the generation of bending angle. The motion monitoring and perception experiments on human body and joints by MAF and D-MAF sensors were further investigated. Fig. 8e–i displayed the potential application of this piezoresistive sensor as a smart clothing. When MAF and D-MAF sensors were attached to the index finger joint, wrist, elbow, knee and vamp, the bending angle was 39°, 21°, 42°, 21° and 34°, respectively. The sensor can detect the corresponding motion and feedback in time. In conclusion, the as-prepared smart sensor with high sensitivity, excellent sensing performance, and cyclic stability presented potential applications for monitoring and analyzing human motions. In comparison to the traditional wearable devices, the present fabric showed higher strength and unique non-tensile sensing behavior. Moreover, the intrinsic soft magnetic characteristics also enable them to be applied in non-contacted magnetic sensing and actuation, thus possessed high potential in modern electronic devices.

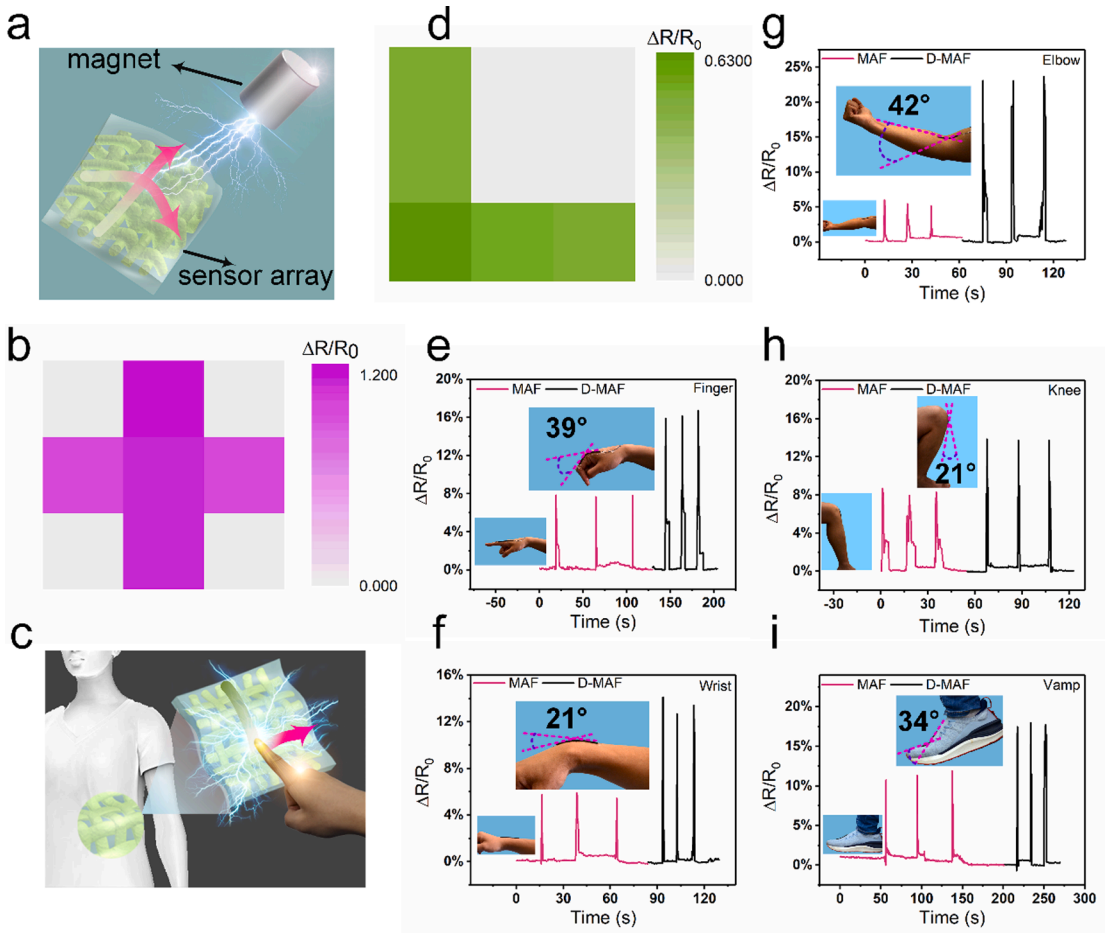

Fig. 8. AFs were woven to form a block fiber network structure (AFs-N), and then encapsulated by MRE (MAF-N). MAF-N sensor array attracted by permanent magnet: (a) Schematic diagram and (b) $\Delta R/R_0$; (c) Potential application in clothing fabrics and (d) pressing the "L" on the MAF-N sensor array with a 10 g weight; Monitor the $\Delta R/R_0$ of human joint bending: (e) forefinger root, (f) wrist, (g) elbow, (h) knee and (i) vamp of MAF and D-MAF sensor. (For interpretation of the references to colour in this figure legend, the reader is referred to the web version of this article.)

4. Conclusion

In summary, a novel non-tensile multi-mode MAF piezoresistive sensor with both stiffen fiber core and elastic magnetic shell was developed. The flax fiber was immersed in the AgNWs solution by ultrasonic treatment to form conductive network, and each strands of flax fiber and silver nanowires were firmly in contact with each other. Besides a large tensile stress, the multi-functional piezoresistive sensors based on MAF and D-MAF were demonstrated to have good flexibility and sensitivity under bending stimuli. These multi-functional D-MAF sensors not only had excellent sensing performance, but also possessed good magneto-actuating properties. Moreover, the shapes of the multi-mode D-MAF sensors could be customized. The deflection angle increased with the enhancing of the magnetic field density, which could meet the deflection behaviors at specific angle requirements. AFs could also be woven into arrays to sense external stimuli, and the final MAF and D-MAF sensors could perceive and monitor the human body motion in real time. As a result, owing to the good mechanical strength and sensing performance, the MAF and multi-mode D-MAF sensors show high prospective in smart electronic devices.

CRediT authorship contribution statement

Quan Shu: Conceptualization, Investigation, Writing – original draft. **Tao Hu:** Investigation, Formal analysis. **Zhenbang Xu:** Funding acquisition. **Junshuo Zhang:** Investigation. **Xiwen Fan:** Investigation. **Xinglong Gong:** Methodology, Funding acquisition, Writing – review & editing. **Shouhu Xuan:** Supervision, Project administration, Resources, Funding acquisition, Writing – review & editing.

Declaration of Competing Interest

The authors declare that they have no known competing financial interests or personal relationships that could have appeared to influence the work reported in this paper.

Acknowledgements

Financial supports from the National Natural Science Foundation of China (Grant Nos. 11822209, 12072338, 11972343), the Anhui's Key R&D Program of China (202104a05020009), the Fundamental Research Funds for the Central Universities (WK2480000007) and Joint Fund of USTC-National Synchrotron Radiation Laboratory (KY2090000055) are gratefully acknowledged. This work was partially carried out at the USTC Center for Micro and Nanoscale Research and Fabrication.

Appendix A. Supplementary material

Supplementary data to this article can be found online at https://doi.org/10.1016/j.compositesa.2021.106548.

References

[1] He K, Liu Y, Wang M, Chen G, Jiang Y, Yu J, et al. An artificial somatic reflex arc. Adv Mater 2020;32(4):1905399.
[2] Wang H, Totaro M, Veerapandian S, Ilyas M, Kong M, Jeong U, et al. Folding and bending planar coils for highly precise soft angle sensing. Adv Mater Technol 2020;5(11):2000659.
[3] Wang Z, Meng G, Wang L, Tian L, Chen S, Wu G, et al. Simultaneously enhanced dielectric properties and through-plane thermal conductivity of epoxy composites with alumina and boron nitride nanosheets. Sci Rep 2021;11(1):2495.
[4] Hwang H, Kim Y, Park J-H, Jeong U. 2D percolation design with conductive microparticles for low-strain detection in a stretchable sensor. Adv Funct Mater 2020;30(13):1908514.
[5] Li W, Zhou Y, Wang Y, Jiang L, Ma J, Chen S, et al. Core-sheath fiber-based wearable strain sensor with high stretchability and sensitivity for detecting human motion. Adv Electron Mater 2021;7(1):2000865.
[6] Qi S, Guo H, Fu J, Xie Y, Zhu M, Yu M. 3D printed shape-programmable magneto-active soft matter for biomimetic applications. Compos Sci Technol 2020;188:107973.
[7] Gao F, Zhang N, Fang X, Ma M. Magnetically directed soft actuators driven by moisture. J Mater Chem C 2017;5(17):4129–33.
[8] Song Y, Min J, Gao W. Wearable and implantable electronics: moving toward precision therapy. ACS Nano 2019;13(11):12280–6.
[9] Yang X, Li L, Wang S, Lu Q, Bai Y, Sun F, et al. Ultrathin, stretchable, and breathable epidermal electronics based on a facile bubble blowing method. Adv Electron Mater 2020;6(11):2000306.
[10] Zhou X, Jia Z, Zhang X, Wang B, Wu W, Liu X, et al. Controllable synthesis of Ni/NiO@porous carbon hybrid composites towards remarkable electromagnetic wave absorption and wide absorption bandwidth. J Mater Sci Technol 2021;87:120–32.
[11] Hou T, Jia Z, Wang B, Li H, Liu X, Bi L, et al. MXene-based accordion 2D hybrid structure with Co_9S_8/C/$Ti_3C_2T_x$ as efficient electromagnetic wave absorber. Chem Eng J 2021;414:128875.
[12] Gao X, Jia Z, Wang B, Wu X, Sun T, Liu X, et al. Synthesis of NiCo-LDH/MXene hybrids with abundant heterojunction surfaces as a lightweight electromagnetic wave absorber. Chem Eng J 2021;419:130019.
[13] Čibiraitė-Lukenskienė D, Ikamas K, Lisauskas T, Krozer V, Roskos HG, Lisauskas A. Passive detection and imaging of human body radiation using an uncooled field-effect transistor-based THz detector. Sensors 2020;20(15):4087.
[14] Fakih I, Durnan O, Mahvash F, Napal I, Centeno A, Zurutuza A, et al. Selective ion sensing with high resolution large area graphene field effect transistor arrays. Nat Commun 2020;11:3226.
[15] Marimuthu G, Nguyen B-S, Pham V-T, Nguyen V-H, Tran V-M, Sivashanmugan K, et al. Novel $NiCo_2O_4$/MWCNTs nanocomposite with flake-like architecture as room temperature capacitive-type NH_3 gas sensor. Mater Lett 2021;283:128814.
[16] Hourlier-Fargette A, Schon S, Xue Y, Avila R, Li W, Gao Y, et al. Skin-interfaced soft microfluidic systems with modular and reusable electronics for in situ capacitive sensing of sweat loss, rate and conductivity. Lab Chip 2020;20(23):4391–403.
[17] Lu Y, Cheng Z, Chen J, Li W, Zhang S. High sensitivity face shear magneto-electric composite array for weak magnetic field sensing. J Appl Phys 2020;128(6):064102.
[18] Wang Y, Luo C, Wang S, Chen C, Yuan G, Luo H, et al. Large piezoelectricity in ternary lead-free single crystals. Adv Electron Mater 2020;6(1):1900949.
[19] Chen Y, Yu M, Bruck HA, Smela E. Compliant multi-layer tactile sensing for enhanced identification of human touch. Smart Mater Struct 2018;27(12):125009.
[20] Qi K, Zhou Y, Ou K, Dai Y, You X, Wang H, et al. Weavable and stretchable piezoresistive carbon nanotubes-embedded nanofiber sensing yarns for highly sensitive and multimodal wearable textile sensor. Carbon 2020;170:464–76.
[21] Lee Y, Myoung J, Cho S, Park J, Kim J, Lee H, et al. Bioinspired gradient conductivity and stiffness for ultrasensitive electronic skins. ACS Nano 2021;15:1795–804.
[22] Al-Handarish Y, Omisore OM, Duan W, Chen J, Zebang L, Akinyemi TO, et al. Facile fabrication of 3D porous sponges coated with synergistic carbon black/multiwalled carbon nanotubes for tactile sensing applications. Nanomaterials 2020;10(10):1941.
[23] Ding X, Zhong W, Jiang H, Li M, Chen Y, Lu Y, et al. Highly accurate wearable piezoresistive sensors without tension disturbance based on weaved conductive yarn. ACS Appl Mater Inter 2020;12(31):35638–46.
[24] Xia T, Yu R, Yuan J, Yi C, Ma L, Liu F, et al. Ultrahigh sensitivity flexible pressure sensors based on 3D-printed hollow microstructures for electronic skins. Adv Mater Technol 2021;6(3):2000984.
[25] Yu Z, Qin B, Ma Z, Huang J, Li S, Zhao H, et al. Superelastic hard carbon nanofiber aerogels. Adv Mater 2019;31(23):1900651.
[26] Ge J, Sun L, Zhang F, Zhang Y, Shi L, Zhao H, et al. A stretchable electronic Fabric artificial skin with pressure-, lateral strain-, and flexion-sensitive properties. Adv Mater 2016;28(4):722–8.
[27] Maschmann MR, Ehlert GJ, Dickinson BT, Phillips DM, Ray CW, Reich GW, et al. Bioinspired carbon nanotube fuzzy fiber hair sensor for air-flow detection. Adv Mater 2014;26(20):3230–4.
[28] Georgopoulou A, Michel S, Vanderborght B, Clemens F. Piezoresistive sensor fiber composites based on silicone elastomers for the monitoring of the position of a robot arm. Sensor Actuat A – Phys 2021;318:112433.
[29] Irfan MS, Khan T, Hussain T, Liao K, Umer R. Carbon coated piezoresistive fiber sensors: From process monitoring to structural health monitoring of composites- A review. Compos Part A-Appl S 2021;141:106236.
[30] Ding L, Xuan S, Feng J, Gong X. Magnetic/conductive composite fibre: A multifunctional strain sensor with magnetically driven property. Compos Part A-Appl S 2017;100:97–105.
[31] Park CS, Kang BS, Lee DW, Choi YS. Single carbon fiber as a sensing element in pressure sensors. Appl Phys Lett 2006;89(22):223516.
[32] Huang S, Feng C, Mayes ELH, Yao B, He Z, Asadi S, et al. In situ synthesis of silver nanowire gel and its super-elastic composite foams. Nanoscale 2020;12(38):19861–9.
[33] Liu X, Liang X, Lin Z, Lei Z, Xiong Y, Hu Y, et al. Highly sensitive and stretchable strain sensor based on a synergistic hybrid conductive network. ACS Appl Mater Inter 2020;12(37):42420–9.
[34] Georgopoulou A, Sebastian T, Clemens F. Thermoplastic elastomer composite filaments for strain sensing applications extruded with an FDM 3D printer. Flex Print Electron 2020;5:35002.
[35] Pan M, Yuan C, Anpalagan H, Plummer A, Zou J, Zhang J, et al. Soft controllable carbon fibre-based piezoresistive self-sensing actuators. Actuators 2020;9(3):79.
[36] Liu M, Zhang S, Liu S, Cao S, Wang S, Bai L, et al. CNT/STF/Kevlar-based wearable electronic textile with excellent anti-impact and sensing performance. Compos Part A-Appl S 2019;126:105612.
[37] Wang H, Wang H, Wang Y, Su X, Wang C, Zhang M, et al. Laser writing of Janus graphene/Kevlar textile for intelligent protective clothing. ACS Nano 2020;14(3):3219–26.
[38] Costa SM, Ferreira DP, Ferreira A, Vaz F, Fangueiro R. Multifunctional flax fibres based on the combined effect of silver and Zinc Oxide (Ag/ZnO) nanostructures. Nanomaterials 2018;8(12):1069.
[39] Tripathi KM, Vincent F, Castro M, Feller JF. Flax fibers-epoxy with embedded nanocomposite sensors to design lightweight smart bio-composites. Nanocomposites 2016;2(3):125–34.
[40] Zhang L, Li H, Lai X, Gao T, Liao X, Chen W, et al. Carbonized cotton fabric-based multilayer piezoresistive pressure sensors. Cellulose 2019;26(8):5001–14.
[41] Liu Z, Chen K, Fernando A, Gao Y, Li G, Jin L, et al. Permeable graphited hemp fabrics-based, wearing-comfortable pressure sensors for monitoring human activities. Chem Eng J 2021;403:126191.
[42] Yang C, Gu H, Lin W, Yuen M, Wong C, Xiong M, et al. Silver nanowires: from scalable synthesis to recyclable foldable electronics. Adv Mater 2011;23(27):3052–6.